

Light reflection from sea ice during the onset of melt

Donald K. Perovich

U.S. Army Cold Regions Research and Engineering Laboratory, Hanover, New Hampshire

Abstract. A knowledge of the reflection of light from a sea ice cover is important for the interpretation of remote sensing imagery at visible and near-infrared wavelengths, for climatological studies involving the energy balance of the polar regions, and for understanding radiative transfer in sea ice. Spectral measurements of albedo, bidirectional reflectance distribution function, and polarized reflectance were made for Arctic sea ice conditions found during the onset of melt. The wavelength region studied was from the visible to the near infrared (400–1000 nm). Results are presented for the five following surface types: (1) dry snow, (2) dry snow with a glazed surface, (3) bare ice, (4) blue ice, and (5) melt pond. Results indicate that spectral albedos decrease at all wavelengths as the melt season progresses and the surface conditions evolve from (1) through (5) and that the decrease is most pronounced at longer wavelengths. Reflectance data suggest that at most angles, reflectance has the same spectral shape as albedo; at 30° zenith, reflectance is for the most part azimuthally isotropic; and at 60° zenith there is a significant specular component at 0° azimuth, especially for the bare ice cases. Light reflected at 60° zenith angle was strongly polarized. In general, light reflected from snow-free ice was more strongly polarized, with the degree of polarization increasing with wavelength.

Introduction

An understanding of the reflection of visible and near-infrared light from a sea ice cover is important for climatological studies involving the energy balance of the polar regions, for the interpretation of remote sensing imagery, and for understanding radiative transfer processes in sea ice. In particular, shortwave radiation plays a critical role in the summer decay of sea ice, and the fraction of the incident irradiance that is reflected by the ice, the albedo, has a major impact on the heat and mass balance of the ice cover [Maykut and Untersteiner, 1971; Untersteiner, 1986]. More recent efforts [Ebert and Curry, 1993] have established the importance of the spectral and angular details of the incident and reflected radiation field to thermodynamic sea ice models. With increased interest in climatological studies there is a need for spatial and temporal information on large-scale ice pack albedos. Satellite data from visible and near-infrared sensors, such as advanced very high resolution radiometer (AVHRR) and thematic mapper, provide a potential source of this information [Steffen *et al.*, 1993].

Because of this impact, spectral and wavelength-integrated albedos have been measured for a wide range of ice types and conditions [Langleben, 1969, 1971; Perovich *et al.*, 1986]. Ice albedos have been found to be sensitive to surface conditions [Grenfell and Maykut, 1977; Grenfell and Perovich, 1984], to the number of air bubbles in the ice [Grenfell, 1983], and to the amount and distribution of brine in the interior of the ice [Perovich and Grenfell, 1981]. Previous work has demonstrated that there can be large seasonal changes in albedo during the onset of summer melt [Grenfell and Perovich, 1984] and during fall freeze-up [Perovich, 1991].

This paper is not subject to U.S. copyright. Published in 1994 by the American Geophysical Union.

Paper number 93JC03397.

There are limitations, however, in applying this large albedo database to the interpretation and application of remotely sensed data. Remote sensing instruments typically have narrow fields of view and thus do not measure the reflected irradiance but rather, the reflected radiance at a particular angle [Taylor and Stowe, 1984]. For satellite sensors at visible and near-infrared wavelengths, surface observations can only be made under clear skies. In this case the reflected radiance field may not be isotropic, increasing the difficulty of converting satellite-observed reflected radiance to the climatological parameter of interest; surface albedo. This also limits the suitability of surface-based albedo measurements in interpreting satellite data to distinguish different ice types.

What is needed is information on the bidirectional reflectance distribution function (BRDF), which is the angular distribution of reflected radiance as a function of solar incidence angle. There have been several studies of BRDFs for snow [Dirnhirn and Eaton, 1975; Kuhn, 1985; Steffen, 1987; Dozier *et al.*, 1988] which are germane to snow-covered sea ice. Field observations of BRDF over lake ice have also been reported [Leshkevich *et al.*, 1990; Bolsenga, 1983]. Because of the significant structural differences between ice grown from freshwater and ice grown from seawater, lake ice optical measurements are only relevant to desalinated and retextured sea ice types, such as refrozen melt ponds. However, BRDF data for sea ice are limited. Schlosser [1988] found that thin sea ice exhibited a strong degree of azimuthal anisotropy that decreased as the ice grew thicker. Perovich [1991] reported BRDF data for a refrozen melt pond and for 0.2-m-thick young ice and found that at azimuths of 0° and 90° from solar incidence, reflectances were relatively constant for zenith angles from 0° to 50°, then increased sharply for larger angles.

Even with albedo and BRDF measurements, discrimination between certain ice types is difficult. While in many

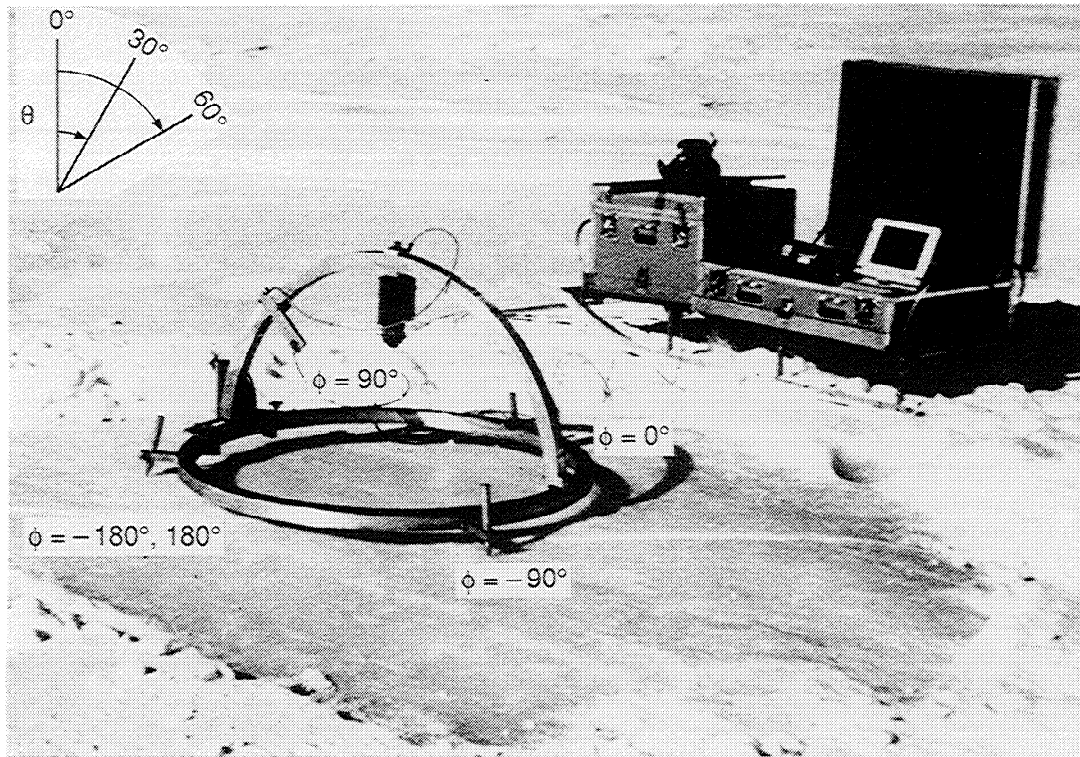


Figure 1. Experimental setup for reflectance measurements. The insulated boxes on the sled contained the spectroradiometer controller and the datalogging notebook computer. The detector was mounted on the metal arch, which could be rotated to any zenith or azimuth angle. Measurements were being made of bare ice. The convention for the zenith θ and azimuth ϕ angles is superposed on the photograph.

cases the reflectance differences are so large, ice types are easy to differentiate, there are others, such as melting snow and white ice, for which that is not the case. Polarization information about the reflected light provides additional information that may be useful in ice type discrimination.

The greatest variety in ice conditions, and consequently, in albedo and reflected radiance, occurs during the onset of summer melt. This paper discusses an optical experiment investigating light reflection from first-year sea ice as it evolved from cold, dry conditions to warm, melting ice. Spectral values of albedo, bidirectional reflectance, and linear polarization are presented for the five following surface types: (1) dry snow, (2) dry snow with a glazed surface, (3) bare ice, (4) blue ice, and (5) melt pond. Each set of measurements was made under clear skies for a single solar incidence angle. Though these are only five specific cases found in a small area, they are, in a general sense, representative of much of the Arctic during the initial stages of summer melt.

Field Experiment

The field program was conducted at Resolute Bay (75°N, 95°W) in the Canadian Archipelago from May 15 to June 9, 1991, during the onset of summer melt. The observation site was in shore-fast, first-year ice. Before the onset of melt the ice was fairly uniform both in thickness and structure. However, because of wind transport, snow depths varied considerably, ranging from 0 to 0.2 m. As the melt season progressed, this uniform ice cover became more diverse.

During the course of the experiment, five distinct surface types were found to be present within an area of less than half a square kilometer; (1) ice covered by dry snow, (2) ice covered by dry snow with a glazed surface, (3) bare ice, (4) blue ice, and (5) a melt pond. For each of these five ice types, spectral measurements were made of the albedo, the angular distribution of the reflected light, and the linear polarization of the reflected light.

The optical measurements were made using a Spectron Engineering SE590 data-logging spectroradiometer. The detector uses a diffraction grating to disperse the spectrum, which is then imaged onto a 256-element silicon photodiode array. The wavelength range of the instrument is 370 to 1100 nm, and it has a full-width, half-power spectral resolution of 8 nm. Low light levels at the extreme ends of the spectrum limited the usable wavelength region to 400 to 1000 nm. The instrument samples the entire spectrum simultaneously, with integration times ranging from 1/60 to 8 s, depending on ambient light levels and the level of precision desired. Output from the instrument was downloaded directly into a notebook computer. Because of the cold conditions and the need for portability, the computer and the instrument control electronics were housed in a sled-mounted, thermally insulated box. The box and sled arrangement, along with the device for measuring reflected radiance, is shown in Figure 1.

To measure albedos, a hemispherical diffuser was placed on the instrument. The angular response of the diffuser was within 8% of cosine for zenith angles from 0° to 80°. The

detector was mounted on a 1.5-m rod to minimize shadowing of the surface. By pointing the detector upward and downward, we measured spectral incident $F_i(\lambda)$ and reflected $F_r(\lambda)$ irradiances, from which spectral albedos $\alpha(\lambda) = F_r(\lambda)/F_i(\lambda)$ were computed. A complete set of spectral albedo measurements took less than 30 s to obtain.

A 1° field of view lens was mounted on the detector for the bidirectional reflectance measurements. The detector was mounted on the semicircular arc shown in Figure 1. This arc was rotated around the base ring to measure reflected radiance at different azimuths and was tilted for different zenith angles. Measurements were made at zenith angles θ of 0°, 30°, and 60° and azimuth angles ϕ from -180° to 180° at 30° intervals. Zenith angles were measured from vertical with 0° looking straight down at the surface (nadir) and 90° tangent to the surface (Figure 1). An azimuth of 0° is pointing toward the sun, while -180° and 180° are away from the sun. Reference values of reflected radiance from a Spectralon white (reflectance = 0.98–0.99) Lambertian reflectance standard were recorded at the beginning and end of each measurement set to monitor changes in the incident irradiance. The change in incident radiance during the 15 min it took to make a set of measurements was typically less than a few percent. A complete determination of the BRDF would entail measuring the zenith and azimuth dependence of reflected radiance for a complete set of solar zenith angles and azimuths. However, this was not practical under field conditions. Measurements were made at only one solar zenith angle between 50° and 60° for each ice type. Since the surfaces studied were flat and free of azimuthally oriented features, the BRDF does not vary with solar azimuth. In this case the BRDF reduces to

$$R(\theta_0, \theta, \phi, \lambda) = dI_r(\theta, \phi, \lambda)/\mu_0 dF_0(\theta_0, \phi, \lambda) \quad (1)$$

where θ_0 is the solar zenith angle, θ and ϕ are the detector zenith and azimuth angles, $\mu_0 = \cos(\theta_0)$, $I_r(\theta, \phi, \lambda)$ is reflected spectral radiance, $F_0(\theta_0, \phi, \lambda)$ is the incident spectral irradiance, and the units are steradians⁻¹ [Warren, 1982]. The BRDF measurements were made on clear, sunny days with the direct beam solar component free of any obscuring clouds. Formally, the BRDF is a derivative quantity, similar in a sense to a probability density function, which being defined in terms of infinitesimal solid angles can not be measured directly. This paper follows the common practical convention of extending the definition of BRDF to encompass ΔI_r and ΔF_0 , as well as dI_r and dF_0 . In these measurements, ΔF_0 included the diffuse sky component as well as the direct solar beam. The bidirectional reflectance factor, $R_f(\theta_0, \phi, \lambda) = \pi R(\theta_0, \phi, \lambda)$, was computed by normalizing the observed reflected radiance from the surface by the reflected radiance from the Spectralon standard. From the BRDF and the albedo measurements the anisotropic reflectance function f

$$f(\theta_0, \phi, \lambda) = \pi R(\theta, \phi, \lambda)/\alpha_0(\theta_0, \lambda)$$

was also computed. This factor provides a direct comparison of reflectance with hemispherically integrated albedo.

The linear polarization of the reflected radiance was also measured. Polarization measurements were made at 0° azimuth for zenith angles of 0°, 30°, and 60° and also at 180° azimuth, 30° zenith. A polarizing element was placed on the 1° field of view lens, and the axis of rotation of the polarizer

was rotated from -90° to 90° in 30° steps. Because of alignment difficulties, polarization angles were accurate only to within 10°. A calibration correction was applied to the polarization results to offset the polarization caused by the instrument.

An important supplement to the optical measurements was a characterization of the physical properties of the snow and sea ice. For the snow this characterization consisted of the depth, vertical profiles of temperature and density, and a description of the grain size and type. Surface conditions were photographed and qualitatively described. The interior of the ice was characterized by analyzing 100-mm-diameter cores taken from the ice. Vertical profiles of temperature, salinity, and brine volume were obtained from the cores. Horizontal and vertical thin sections were prepared from the ice cores to determine crystal types and sizes and to ascertain the size distribution of air and brine inclusions.

Results

Physical Properties

The five cases examined in this paper represent ice types commonly present during the initial stages of summer melt. Before melt begins there is only one ice type present from an optical perspective; snow-covered ice. At this stage the underlying ice was relatively uniform, with a thickness of approximately 1.6 m and salinity ranging from 6 to 8‰. Since the ice was still cold, brine volumes were relatively low, 5% or less. The ice crystallography was horizontally homogeneous, with the top few centimeters of the ice cover being granular and the remainder columnar with the c axis in the horizontal plane. Once melt began, the ice conditions quickly became more variable. Differences in snow depth caused variation in the progression of the melt. Though the ice cover was fairly flat initially, some small-scale topography began to develop as melting progressed. Brine drainage tended to be greater in high areas, resulting in bubbly ice, while some of the low regions became sites of melt ponds. Selected physical properties and optical results are summarized in Table 1 for the five cases.

The snow-covered ice case consisted of 0.23 m of snow with three distinct stratigraphic layers. There was a 0.03-m-deep surface layer of fluffy new snow composed of 0.5-mm-to 1-mm-diameter plates with a density of 180 kg/m³. Under that was a 0.17-m, hard-packed wind slab with 0.5-mm rounded grains and a density of 400 kg/m³. The bottom layer was 0.03 m of depth hoar with 2-mm scrolls and a density of 300 kg/m³. The snow cover was optically thick, so the contribution of the underlying ice to the reflected light was negligible. For the glazed snow case the stratigraphy of the bottom two layers was similar, with a depth hoar layer covered by a wind slab. The difference from the snow case was in the surface layer. Instead of new snow there was a hard, glazed surface a few millimeters thick. The glazed snow cover was also optically thick with a total depth of 0.24 m.

In the bare ice case the top 0.05 m of the ice was quite bubbly and looked milky white. There was also a distinct bubble band from 0.09 to 0.11 m deep with scattered bubbles to 0.29 m. The remainder of the ice was relatively bubble-free. The bubbly surface layer resulted from the brine pockets draining, which left air voids behind. The blue ice was quite similar to the bare ice, except for the surface layer.

Table 1. Summary of Selected Ice Physical Properties and Optical Results

	Surface Type				
	Snow	Glazed Snow	Bare Ice	Blue Ice	Melt Pond
<i>Physical Properties</i>					
Solar elevation angle	56	58	60	58	52
Ice thickness, m	1.60	1.50	1.58	1.58	1.55
Snow depth, m	0.23	0.24	0.00	0.00	0.00
<i>Optical Results, 450 nm</i>					
Albedo	0.97	0.84	0.78	0.69	0.43
$R_f(0)$	0.96	0.98	0.71	0.64	0.40
$R_f(30, 0)$	1.03	1.18	0.77	0.77	0.44
$R_f(30, 90)$	0.94	0.95	0.74	0.66	0.36
$R_f(30, 180)$	0.93	0.96	0.74	0.63	0.37
$R_f(60, 0)$	1.32	1.48	1.68	1.14	0.61
$R_f(60, 90)$	0.93	0.95	0.78	0.70	0.38
$R_f(60, 180)$	0.80	0.44	0.44	0.57	0.36
$f(0)$	0.99	1.18	0.91	0.93	0.93
$f(30, 0)$	1.06	1.41	0.99	1.12	1.04
$f(30, 90)$	0.97	1.14	0.95	0.96	0.84
$f(30, 180)$	0.96	1.14	0.95	0.91	0.86
$f(60, 0)$	1.36	1.77	2.16	1.66	1.42
$f(60, 90)$	0.96	1.14	1.01	1.02	0.89
$f(60, 180)$	0.82	0.53	0.56	0.83	0.83
$DP(0)$	-0.007	-0.014	-0.008	-0.012	...
$DP(30, 0)$	-0.003	-0.007	0.002	-0.023	...
$DP(60, 0)$	0.045	0.235	0.321	0.251	...
$DP(30, 180)$	0.016	0.029	0.024	0.011	...
<i>Optical Results, 950 nm</i>					
Albedo	0.87	0.70	0.47	0.33	0.10
$R_f(0)$	0.84	0.72	0.30	0.26	0.03
$R_f(30, 0)$	0.92	1.04	0.41	0.44	0.06
$R_f(30, 90)$	0.83	0.84	0.38	0.33	0.03
$R_f(30, 180)$	0.82	0.72	0.35	0.25	0.03
$R_f(60, 0)$	1.37	1.66	1.48	0.78	0.14
$R_f(60, 90)$	0.82	0.83	0.41	0.33	0.02
$R_f(60, 180)$	0.74	0.18	0.13	0.21	0.02
$f(0)$	0.97	1.03	0.63	0.79	0.29
$f(30, 0)$	1.07	1.48	0.86	1.36	0.64
$f(30, 90)$	0.96	1.20	0.80	1.01	0.31
$f(30, 180)$	0.95	1.03	0.75	0.76	0.29
$f(60, 0)$	1.58	2.38	3.12	2.39	1.47
$f(60, 90)$	0.95	1.19	0.87	1.01	0.20
$f(60, 180)$	0.86	0.26	0.27	0.64	0.20
$DP(0)$	0.007	0.007	-0.010	0.054	...
$DP(30, 0)$	-0.018	-0.067	-0.058	-0.104	...
$DP(60, 0)$	0.051	0.226	0.415	0.538	...
$DP(30, 180)$	0.018	0.031	-0.010	-0.063	...

Numbers in parentheses following albedos, reflectance factors R_f , anisotropic reflectance factors f , and degree of polarization DP are selected elevation and azimuth angles (θ , φ), respectively.

The top of the blue ice had significantly fewer bubbles, giving the ice more of a bluish appearance. Ice temperatures, salinities, and brine volumes in the remainder of the bare ice and blue ice were quite similar. The melt pond was shallow, with only 0.03 m of water over 1.55 m of ice. The melt pond had warmed considerably and was nearly isothermal, with temperatures near -1.5°C . Because of the moderate temperatures, brine volumes were large, of the order of 20%.

Desalination was evident in the melt pond case, with ice salinities of a few parts per thousand. However, unlike the bare ice case, brine drainage did not result in a bubbly ice layer due to the presence of the surface water.

Spectral Albedos

Spectral albedos for the five cases are displayed in Figure 2a. The highest albedos are for the snow-covered ice, where visible values are as high as 0.95. Replacing the top few centimeters of new snow with a thin surface glaze results in a reduction of 0.1 to 0.2 in albedo across the spectrum. For both snow cases, albedos were uniform across the visible portion of the spectrum, giving the snow a white appearance. Comparing the bare ice with the blue ice illustrates the impact of a relatively thin (0.04 m) bubbly surface layer. Albedos for the bare ice with the bubbly layer are 0.1 to 0.3 larger than those for the blue ice, with the largest increase between 700 and 800 nm. There is a sharp decrease in albedo associated with ponding of the ice surface. Spectral variations in albedo are more pronounced for the melt pond, with values decreasing from 0.4 at 500 nm to 0.15 at 750 nm, giving the ponds a blue appearance. The observed albedos are consistent with those reported in previous studies [Grenfell and Maykut, 1977; Perovich *et al.*, 1986].

The spectral reflectance factor at nadir, $R_f(\theta_0, 0^\circ, 0^\circ, \lambda)$, is plotted for the five cases in Figure 2b. Comparing these results with those in Figure 2a is instructive since it shows how reflectances from a directly downward looking sensor compare to albedo values. The general spectral shape of the curves in Figures 2a and 2b is similar for individual ice types. For the glazed snow case, nadir reflectance factors are significantly (0.1–0.15) larger than albedos at visible wavelengths. In fact, at visible wavelengths the glazed snow reflectances are slightly larger than the snow values. Anisotropic reflectance factors f are plotted in Figure 2c to highlight differences between hemispherical albedo and reflectance. For the snow case, values of f are near 1 and are constant with wavelength, while f decreases with increasing wavelength for the other four cases. This decrease is most pronounced for the melt pond case, where f drops from 0.95 at 400 nm to 0.25 at 1000 nm. Albedos, reflectance factors, and anisotropic reflectance factors are compared at 450 and 950 nm in Table 1. At 450 nm, values are within 10%, except for the glazed snow, where reflectances are 15% larger. Bare ice, blue ice, and ponded ice all show nadir reflectance factors substantially smaller than albedos at 950 nm, with the percent decrease being greatest for the ponded ice.

Bidirectional Reflectance Distribution Functions

Spectral values of the bidirectional reflectance factor are plotted in Figure 3 for the bare ice case, with albedos plotted for comparison. The measurements were made under clear skies with a solar zenith angle of 60° . For all azimuth and zenith angles the reflectance decreases with increasing wavelength from 450 to 950 nm. Examining the data in more spectral detail revealed that the maximum reflectance was near 470 nm, where the absorption coefficient of pure ice has a minimum [Grenfell and Perovich, 1981]. At 30° zenith the azimuthal dependence of reflectance was weak, and values were comparable to albedos (Table 1). There was a pronounced azimuthal dependence for a detector zenith angle of 60° , with a sharp spike in reflectance at 0° azimuth to more than double the

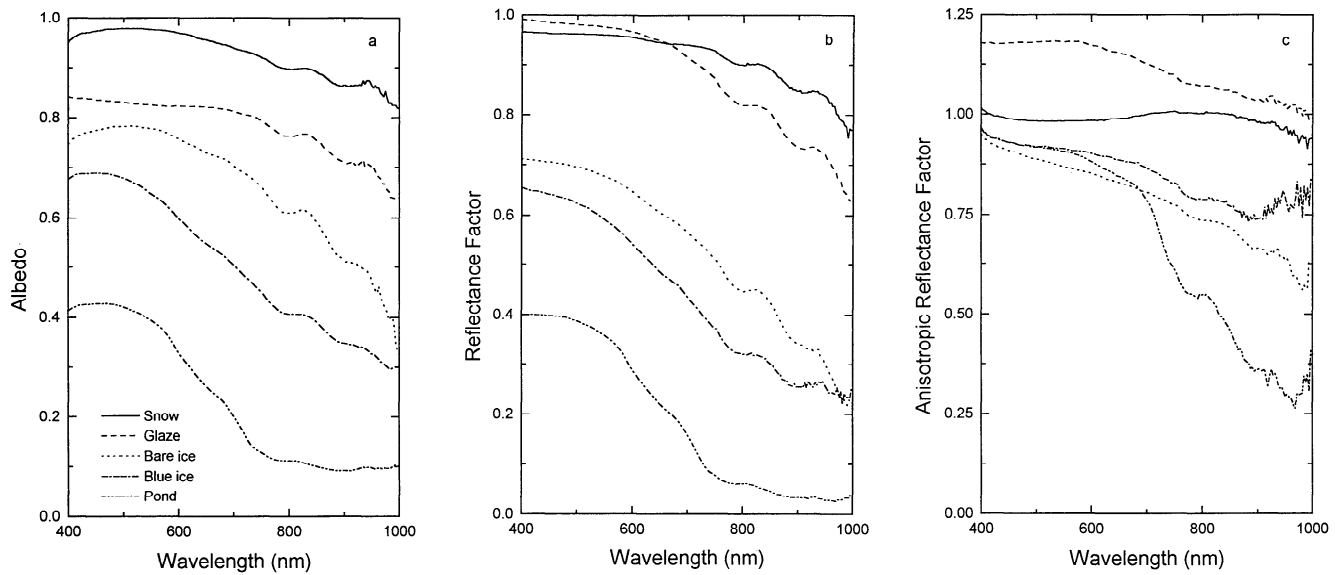


Figure 2. (a) Spectral albedos, (b) reflectance factors at nadir, and (c) anisotropic reflectance factors at nadir for snow-covered ice, glazed snow over ice, bare ice, blue ice, and ponded ice.

albedo. This spike was not surprising since $\theta = 60^\circ$, $\phi = 0^\circ$ was the angle of reflection of the direct solar beam.

Bidirectional reflectance factors at 450 nm for the five ice types are presented in Figure 4a. At 30° zenith the azimuthal dependence is weak for snow, bare ice, blue ice, and the melt pond, with the glazed snow showing significantly enhanced reflectance at an azimuth of 0° . These results are consistent with earlier studies done on refrozen melt ponds and young ice [Perovich, 1991]. All the ice types exhibit azimuthal dependence in reflectance factor at 60° zenith,

with sharp increases at 0° azimuth. Again, this sharp increase is understandable, owing to the large specular contribution at the angle of reflection of the direct solar beam. The azimuthal dependence is weakest for the snow and strongest for the bare ice and the glazed snow surfaces, where the reflectance factor in the forward direction (azimuth = 0°) is more than double that in the backward direction (azimuth = -180° , 180°). The glazed snow and bare ice increases were so great that their reflectance factors at 0° azimuth were larger than values for snow.

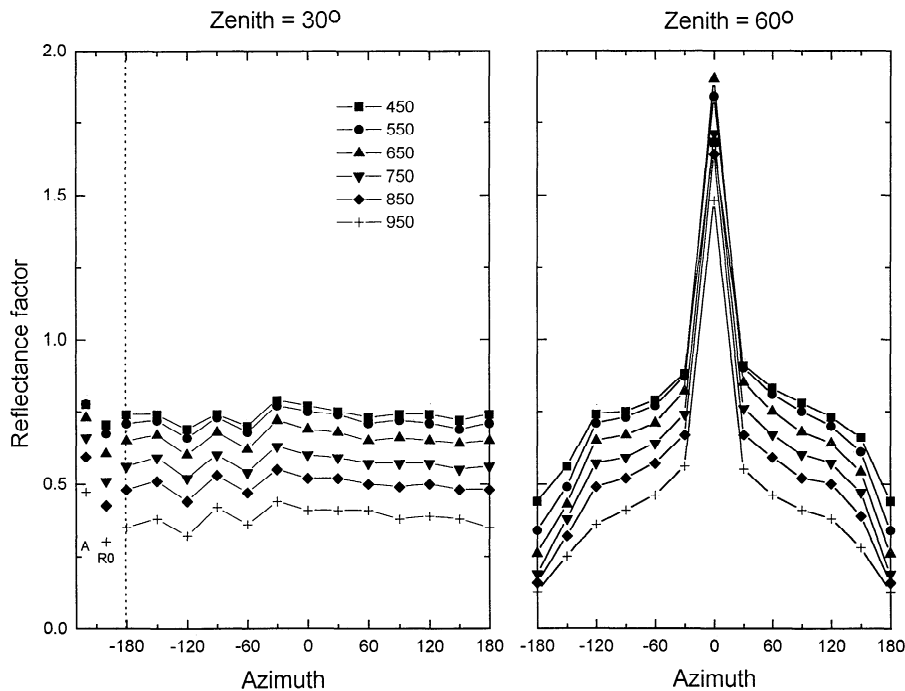


Figure 3. Spectral values of the bidirectional reflectance function for bare ice. The solar incidence angle was 60° . Albedos A and nadir reflectance factors R_0 are plotted on the left-hand side of the dotted line for comparison.

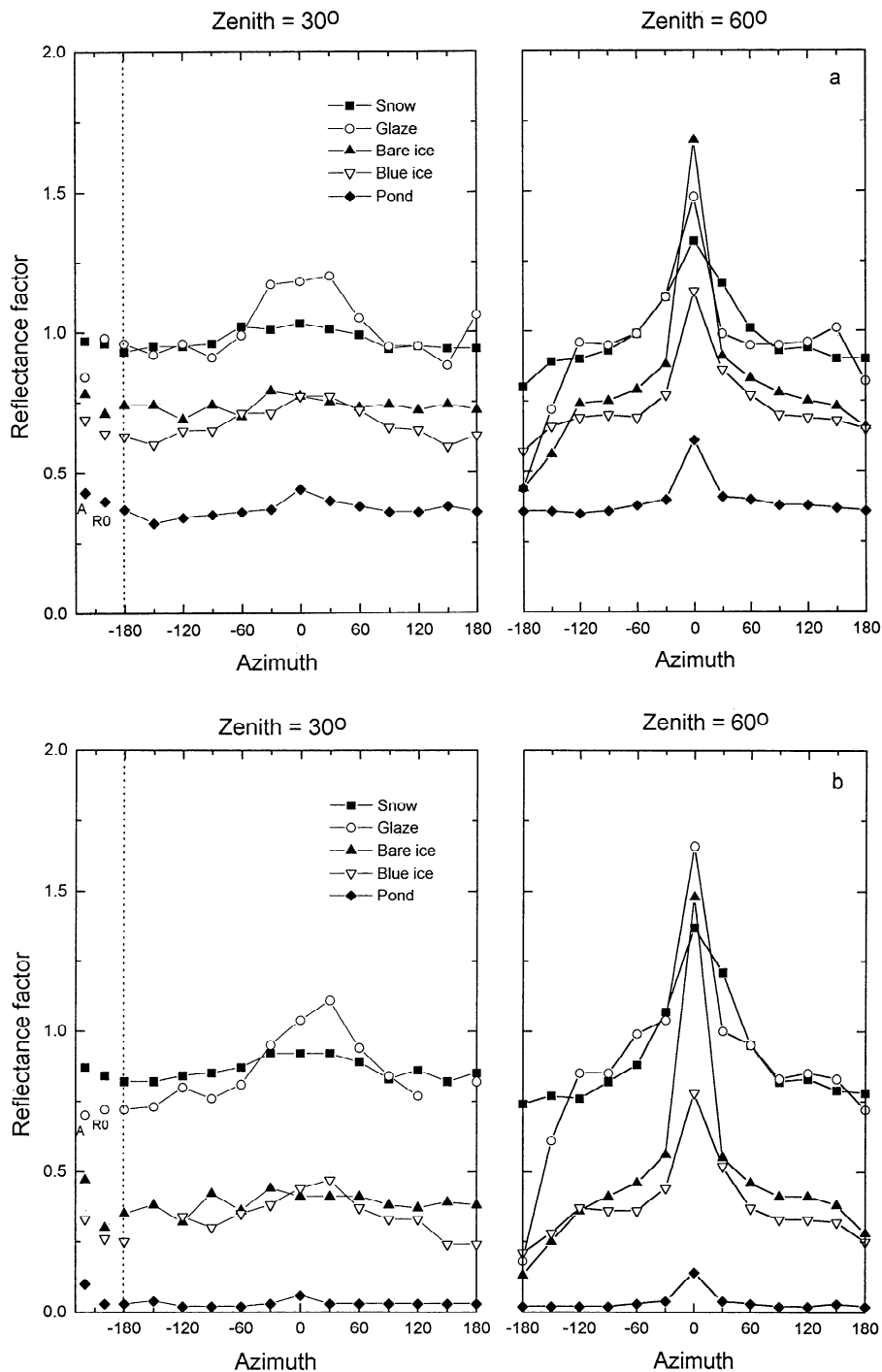


Figure 4. Bidirectional reflectance function for snow-covered ice, glazed snow over ice, bare ice, blue ice, and ponded ice at (a) 450 nm and (b) 950 nm. Albedos A and nadir reflectance factors R_0 are plotted on the left-hand side of the dotted line for comparison.

Bidirectional reflectance factors at 950 nm are presented in Figure 4b to illustrate the wavelength dependence of reflectance. The character of its azimuth dependence is similar to that at 450 nm, though the magnitude of the reflectance factor is reduced, and the azimuthal dependence is stronger. For example, glazed snow and bare ice exhibit more than a threefold increase in reflectance factor from the backward to the forward directions at 60° zenith angle. The stronger azimuthal dependence is not surprising. Absorption in the ice is greater at longer wavelengths [Grenfell and Perovich,

1981], emphasizing the contribution of specular reflection, which is a function of the zenith and azimuth angles.

Initially, it was assumed that the surface was flat and free of azimuthally oriented features. If indeed this was the case, then there should be azimuthal symmetry in reflectance factor between -180° and 0° and 180° and 0° . Within experimental uncertainties this is true for all cases except the glazed snow, where significant asymmetry was evident. Also, the glazed snow was the only case where the anisotropic reflectance factor at nadir was greater than 1. While

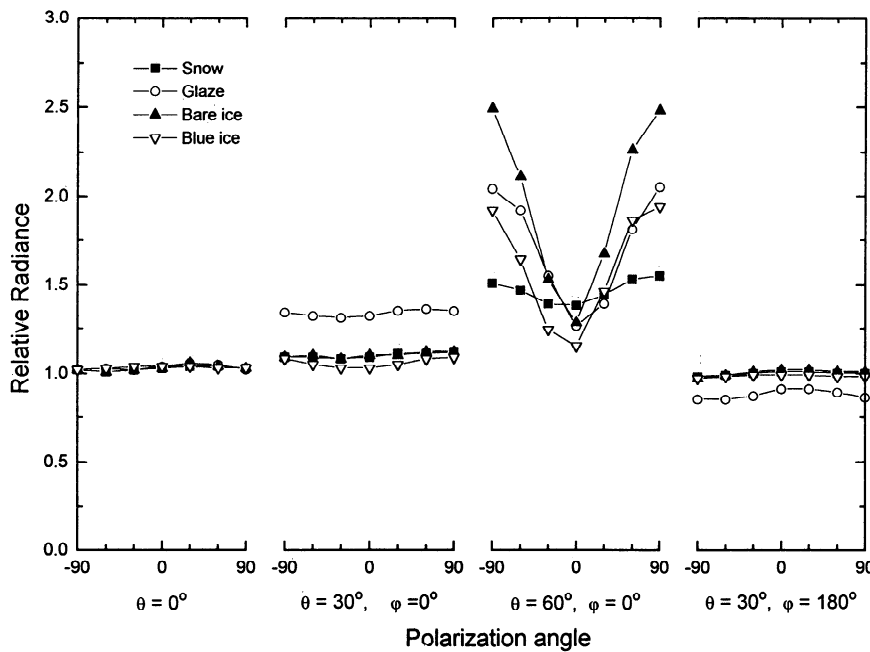


Figure 5. Linear polarization of reflected light at 450 nm for snow, glazed snow, bare ice, and blue ice. Measurements are at 0° azimuth and zenith angles of 0°, 30°, 60° and at 180° azimuth, 30° zenith. All results are normalized to values from -90° polarization (horizontal polarization) and 0° zenith angle.

no detailed surface roughness characterization was performed, photographs show regular bumps a few centimeters high and 10–20 cm across. These roughness elements were responsible for the azimuthal asymmetry in reflectance and the values of $f(0^\circ)$ greater than 1.

There are several difficulties inherent in using satellite-sensed, narrowband reflectance to derive surface albedo. Even after adjusting for atmospheric absorption and discriminating between ice and clouds, there is still the problem of converting a directional reflectance into a hemispherically integrated albedo. The measurements indicate that, with the possible exception of snow, typical ice types are not Lambertian reflectors, particularly at large elevation angles. Thus satellite data must be adjusted with respect to the BRDF of the surface, the solar angle, and the detector angle to accurately estimate the albedo. The anisotropic reflectance factors summarized in Table 1 show the necessity of making these adjustments. For a narrow swath sensor, such as thematic mapper, detector angles are near nadir, and adjustments at short wavelengths are minor. However, in the near-infrared there was significant deviation from isotropic reflection, even at nadir, for the snow-free cases with $f = 0.63$ for bare ice, $f = 0.79$ for blue ice, and $f = 0.29$ for the melt pond. Correcting for anisotropic surface reflectance is even more important for wide swath sensors (e.g., AVHRR) that acquire data using large detector zenith angles. For example, for the bare ice and a detector zenith angle of 60° the anisotropic reflectance factor changes from 0.56 at 180° azimuth to 2.16 at 0° azimuth. At longer wavelengths the change is even greater, with values of f at 950 nm of 0.27 at 180° azimuth and 3.12 at 0° azimuth.

Linear Polarization

The degree of linear polarization of the light reflected from the five ice types was also investigated. Results at 450 nm for

0° azimuth and zenith angles of 0°, 30°, 60°, and -30° are plotted in Figure 5. The data were normalized to the value for horizontally polarized light (-90°) at 0° zenith angle for comparison purposes and are plotted from -90° polarization (horizontal) through 0° (vertical) to 90° (horizontal). The melt pond results were severely compromised by wind-driven ripples on the surface of the pond. Because of this large uncertainty, specific polarization data from the melt pond case are not reported. The pond data do indicate, at least in a qualitative sense, that there was significant polarization of the reflected light, in all likelihood more than for the other ice types.

The most striking feature of Figure 5 is the strong polarization at 60° zenith angle. This is a result of a large specular reflection component plus strong polarization near Brewster's angle. With solar incidence angles between 52° and 60° a detector orientation of 0° azimuth and 60° zenith angle was close to the angle of reflection, where there is a large specular component in the reflected light. Also, near Brewster's angle the specularly reflected light is strongly horizontally polarized. For ice with an index of refraction n_i of 1.31 and air with $n = 1.0$, Brewster's angle = $\tan^{-1}(n_i/n) = 53^\circ$ [Jenkins and White, 1976], which is close to the angle of solar incidence for the observations. Because of the weak wavelength dependence of the index of refraction for ice, Brewster's angle is essentially constant from 400 to 1000 nm. Thus the high polarization at 60° zenith was a direct result of specular reflection at incidence angles near Brewster's angle. The polarization was smallest for the snow, where with its rough, irregular surface, the specular component was small and the reflected light was dominated by volume scattering. At other zenith angles away from Brewster's angle, where the specular component was smaller, there was much less linear polarization of the reflected light. At 0° zenith the reflected light was essentially unpolarized in all

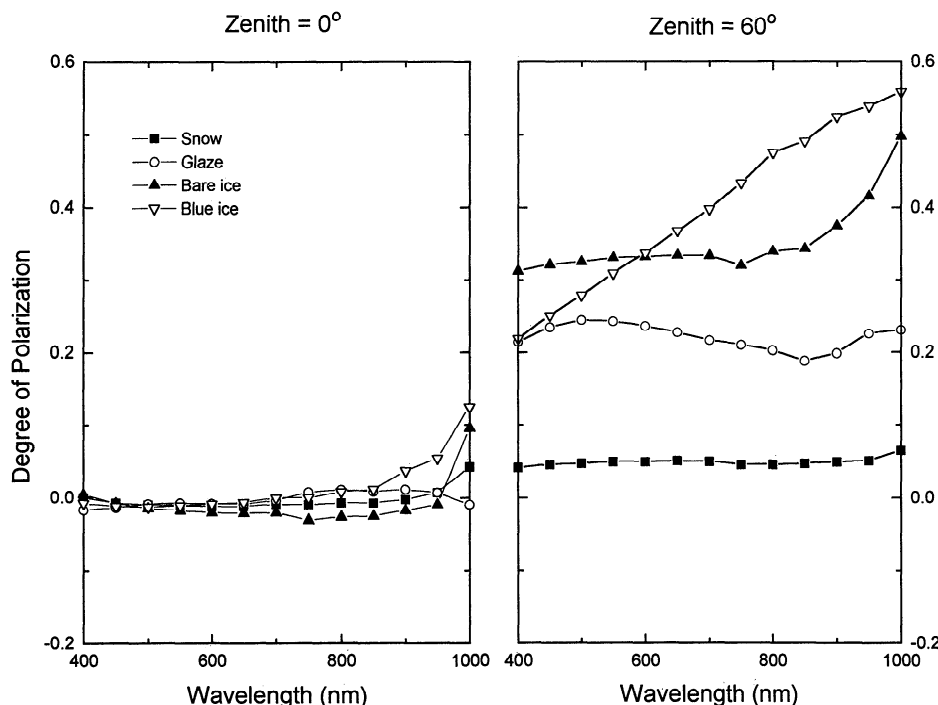


Figure 6. Degree of polarization as a function of wavelength for snow, glazed snow, bare ice, and blue ice at an azimuth of 0° and zenith angles of 0° and 60° .

cases. At 30° and -30° zenith there was a small amount of polarization present for the glazed snow.

The degree of polarization DP for the reflected light is

$$DP = (R_h - R_v)/(R_h + R_v)$$

where R_h and R_v are the horizontal and vertical polarized reflectances [Jenkins and White, 1976]. Results for snow, glazed snow, bare ice, and blue ice at zenith angles of 0° and 60° are plotted in Figure 6. At 0° zenith angle the polarization ratio is near zero and shows little wavelength dependence, though the bare ice and blue ice do show a small increase near 1000 nm. At 60° the polarization ratio is greater than zero for all cases at all wavelengths. There is minimal wavelength dependence for the snow and glazed snow cases, while the bare ice exhibits an increase in DP at longer wavelengths, and the blue ice shows an almost linear increase in DP with wavelength. For the snow-free cases the overall tendency was increased polarization at longer wavelengths. This is consistent with our understanding of radiative transfer in sea ice. The reflected light consists of a surface component and a volume component. The volume contribution is largely unpolarized, while the surface typically is somewhat polarized. Surface reflection is essentially independent of wavelength, while the volume component is reduced at longer wavelengths due to increased absorption in the ice [Grenfell and Perovich, 1981]. The end result is an increase in the degree of polarization with increasing wavelength.

The blue ice case is a good example of this. The ice was vertically homogeneous, with no significant surface scattering layer. Thus the volume contribution to scattering was largely dependent on the light penetration depth, which decreases with increasing wavelength due to increased absorption. The polarized surface reflection component was

independent of wavelength but was sensitive to angle, increasing sharply near $\theta = 60^\circ$, $\phi = 0^\circ$. Therefore the reflected light consisted of a polarized surface component whose magnitude was essentially constant with wavelength and an unpolarized volume component that decreased with wavelength. For most angles, volume scattering dominated, and there was little polarization of the reflected light. However, at angles where the surface component was large and was near Brewster's angle there was considerable polarization of the reflected light, and the degree of polarization increased with wavelength.

Discussion

As the melt season progresses and the surface conditions evolve from dry snow through ponded ice, spectral albedos decrease at all wavelengths. The decrease is most pronounced at longer wavelengths, where the surface layer conditions have a larger impact on the albedo. The BRDF measurements demonstrated that at 0° zenith angle the reflectance factor has the same spectral shape as the albedo. The magnitude of the reflectance factor was roughly comparable to the albedo for dry snow, was 0.10 to 0.15 larger for glazed snow, and was 0.05 to 0.10 smaller for bare ice, blue ice, and ponded ice. At 30° zenith angle the reflectance factor showed little azimuthal dependence, aside from the glazed snow case, where there was an increase at 0° azimuth. When the detector was placed at 60° zenith angle, approximately the solar incidence angle, a pronounced azimuthal dependence was evident for all five ice types, with maximum reflectances at 0° azimuth. The relative increase in reflectance factor at 0° azimuth was greater at longer wavelengths. These results confirm that light reflection from sea ice is quite sensitive to surface conditions. The differences in light

reflection among these five cases are a direct result of differences in the surface conditions and in the physical properties of the top 0.1 to 0.2 m of the ice.

Future observational work should focus on investigating different ice types and extending the polarization measurements. The five ice types presented here represent only a start in characterizing light reflection from sea ice. Additional ice types that need to be examined include young ice, pancake ice, mature melt ponds, refrozen ponds, melting snow, and drained, highly scattering white ice. In addition, surfaces with macroscopic topography, such as sastrugi, ice rubble, and hummocky ice, need to be studied. Further observations made at large solar zenith angles, where the anisotropy of reflectance is expected to be greater, would be valuable. More detailed polarization measurements would be a useful adjunct to future programs. Through measurement of the elliptical and circular polarization, the full polarization state (i.e., the Stokes vector) could be determined.

These observations of light reflection from sea ice can be used to assist in developing and evaluating multistream radiative transfer models [Grenfell, 1991]. Because of the practical difficulties associated with measuring reflectance at all solar incidence and detector angles for all ice types, models are needed to extend the available data to generate complete BRDFs. Results from such models would be of significant value in determining large-scale surface albedos from satellite data. Such models, particularly when combined with spectral data and polarization information, could also provide significant insight into the details of radiative transfer in sea ice.

It is important to consider these results in the context of radiative transfer. Light reflection from snow and ice consists of a specular component and a volume component. The specular component is sensitive to the angle of incidence and reflection, while the volume component depends on the scattering and absorption coefficients of the medium. For sea ice at visible and near-infrared wavelengths the scattering properties can be considered independent of wavelength [Bohren and Huffman, 1983], while absorption increases with increasing wavelength. Thus, in some cases, results at different wavelengths can potentially be combined to obtain information regarding scattering, and therefore ice conditions, at different depths in the upper portion of the ice. Polarization data show promise as a means of differentiating between surface and volume scattering contributions. Detailed spectral reflectance and polarization data such as those reported here could therefore be of potential value in developing inverse models of sea ice radiative transfer. In these models, observed spectral BRDFs and polarizations would be used to generate estimates of the vertical distribution of such physical properties as the air bubbles and brine pockets.

Acknowledgments. The author thanks J. W. Govoni, T. C. Grenfell, and G. Cota for their assistance in the field program and G. Koh for helpful discussions. He also thanks the staff of the Polar Continental Shelf Project at Resolute Bay for their willing and able logistical support. Special thanks to three anonymous reviewers who cleared up some muddled text and thinking. This work was funded by Office of Naval Research contract N0001492MP24006 and Department of the Army project 4A161102AT24.

References

- Bohren, C. F., and Huffman, D. R., *Absorption and Scattering of Light by Small Particles*, John Wiley, New York, 1983.
- Bolsenga, S. J., Spectral reflectances from snow and freshwater ice from 340 to 1100 nm, *J. Glaciol.*, 29, 296–305, 1983.
- Dirmhirn, I., and F. D. Eaton, Some characteristics of the albedo of snow, *J. Appl. Meteorol.*, 14, 375–379, 1975.
- Dozier, J., R. E. Davis, A. T. C. Chang, and K. Brown, The spectral bidirectional reflectance of snow, Proceedings of the 4th International Colloquium on Spectral Signatures of Objects in Remote Sensing, *Eur. Space Agency Spec. Publ.*, ESA SP-287, 87–92, 1988.
- Ebert, E. E., and J. A. Curry, An intermediate one-dimensional thermodynamic sea ice model for investigating ice-atmosphere interactions, *J. Geophys. Res.*, 98, 10,085–10,019, 1993.
- Grenfell, T. C., A theoretical model of the optical properties of sea ice in the visible and near infrared, *J. Geophys. Res.*, 88, 9723–9735, 1983.
- Grenfell, T. C., Radiative transfer model for sea ice with vertical structure variations, *J. Geophys. Res.*, 96, 16,991–17,001, 1991.
- Grenfell, T. C., and G. A. Maykut, The optical properties of ice and snow in the Arctic Basin, *J. Glaciol.*, 18, 445–463, 1977.
- Grenfell, T. C., and D. K. Perovich, Radiation absorption coefficients of polycrystalline ice from 400 to 1400 nm, *J. Geophys. Res.*, 86, 7447–7450, 1981.
- Grenfell, T. C., and D. K. Perovich, Spectral albedos of sea ice and incident solar irradiance in the southern Beaufort Sea, *J. Geophys. Res.*, 89, 3573–3580, 1984.
- Jenkins, F. A., and H. E. White, *Fundamentals of Optics*, McGraw-Hill, New York, 1976.
- Kuhn, M., Bidirectional reflectance of polar and alpine snow surfaces, *Ann. Glaciol.*, 6, 164–167, 1985.
- Langleben, M. P., Albedo and degree of puddling of a melting cover of sea ice, *J. Glaciol.*, 8, 407–412, 1969.
- Langleben, M. P., Albedo of melting sea ice in the southern Beaufort Sea, *J. Glaciol.*, 10, 101–104, 1971.
- Leshkevich, G. A., D. W. Deering, T. F. Eck, and S. P. Ahmad, Diurnal patterns of the bidirectional reflectance of fresh-water ice, *Ann. Glaciol.*, 14, 153–157, 1990.
- Maykut, G. A., and N. Untersteiner, Some results from a time dependent, thermodynamic model of sea ice, *J. Geophys. Res.*, 76, 1550–1575, 1971.
- Perovich, D. K., Seasonal changes in sea ice optical properties during fall freeze-up, *Cold Reg. Sci. Technol.*, 19, 261–273, 1991.
- Perovich, D. K., and T. C. Grenfell, Laboratory studies of the optical properties of young sea ice, *J. Glaciol.*, 27, 331–346, 1981.
- Perovich, D. K., G. A. Maykut, and T. C. Grenfell, Optical properties of ice and snow in the polar oceans, I, Observations, *Ocean Optics 8, Proc. SPIE Int. Sco. Opt. Eng.*, 637, 232–241, 1986.
- Schlosser, E., Optical studies of Antarctic sea ice, *Cold Reg. Sci. Technol.*, 15, 289–293, 1988.
- Steffen, K., Bidirectional reflectance of snow at 500–600 nm, in *Large Scale Effects of Seasonal Snowcover*, *IAHS Publ.*, 166, 415–425, 1987.
- Steffen, K., et al., Snow and ice applications of AVHRR in polar regions: Report of a workshop held in Boulder, Colorado, 20 May 1992, *Ann. Glaciol.*, 17, 1–16, 1993.
- Taylor, V. R., and L. L. Stowe, Reflectance characteristics of uniform earth and cloud surfaces derived from NIMBUS-7 ERB, *J. Geophys. Res.*, 89, 4987–4996, 1984.
- Untersteiner, N., *The Geophysics of Sea Ice*, Plenum, New York, 1986.
- Warren, S. G., Optical properties of snow, *Rev. Geophys.*, 20, 67–89, 1982.

D. K. Perovich, U.S. Army Cold Regions Research and Engineering Laboratory, 72 Lyme Road, Hanover, NH 03755. (e.mail: OMNET)

(Received March 10, 1993; revised November 8, 1993; accepted July 23, 1993.)